Proceedings of the Combustion Institute 42 (2026) 106214

Contents lists available at ScienceDirect

Proceedings of the Combustion Institute

journal homepage: www.elsevier.com/locate/proci

Limit phenomena and kinetic modeling of ammonia fuels in an unstrained diffusion flame burner

Elie Antar [a,b,*], Philippe Versailles [b], Etienne Robert [b]

[a] Department of Mechanical Engineering, McGill University, 817 Sherbrooke Street West, Montreal, Quebec H3A 0C3, Canada
[b] Department of Mechanical Engineering, Polytechnique Montréal, 2500 Chemin de Polytechnique, Montreal, Quebec H3T 1J4, Canada

ARTICLE INFO

Keywords:
Ammonia
Extinction
Instabilities
Diffusion flames
Reaction kinetics

ABSTRACT

A unique experimental facility that can produce nominally unstrained one-dimensional (1D) diffusion flames is used to study the limit phenomena of flame stability and extinction of ammonia (NH_3) blended with varying levels of hydrogen (H_2), methane (CH_4), methanol (CH_3OH), or ethanol (C_2H_5OH). Diffusive–thermal instabilities, including cellular-pulsating flames, are observed prior to extinction. The absence of significant parasitic hydrodynamic effects, omnipresent in common research burners, enables the characterization of the fundamental properties of the instabilities across a wide range of experimental conditions. Extinction is attained by increasing the fraction of inert species (CO_2 or N_2) in the fuel. For all fuel blends, increasing the ammonia fraction is shown to favor extinction, and insights are provided via sensitivity and reaction pathway analyses. The finite-rate chemistry is leveraged to compare 11 thermochemical reaction mechanisms through measured extinction limits. Noticeable discrepancies with the experimental data and among the predictions from the mechanisms are observed.

Novelty and significance statement: Existing experimental data on the limit phenomena of ammonia flames are largely focused on premixed systems, and limited in fuel composition. In this paper, an unstrained diffusion flame burner is used to study more than 70 mixtures of ammonia blended with hydrogen, methane, methanol and ethanol, spanning ammonia fractions from 0 to 100%. Extinction limits are presented, which are of direct relevance to the ongoing efforts to design efficient low-carbon engines, given the inherently low reactivity of ammonia. These measurements also establish a new experimental benchmark for improving ammonia reaction mechanisms, as significant discrepancies are observed among 11 commonly used mechanisms when evaluated in this flame configuration for the first time. Diffusive–thermal flame instabilities, which are typically obscured by parasitic hydrodynamic effects in conventional research burners, are observed prior to extinction. These measurements provide rare experimental access to flame stability behavior in a configuration directly compatible with theoretical flame stability models.

1. Introduction

Interest in ammonia combustion has significantly increased amid the ongoing quest for carbon-neutral alternative fuels [1]. NH_3 has a higher heating value (HHV) that is on par with coal (22.5 MJ/kg), with several studies demonstrating potential for use in internal combustion engines and gas turbines [2,3]. However, compared to more traditional fuels such as natural gas, ammonia is associated with inferior combustion properties, such as low flame speeds, narrow flammability limits, and high ignition energies [4]. A common approach to enhance the combustion of NH_3 is to partially crack it into H_2 and N_2, or blend it with more reactive fuels that can be sourced from biological processes, such as CH_4, CH_3OH, or C_2H_5OH [5], to maintain a low carbon footprint.

Various fundamental aspects of NH_3 combustion have been investigated, including chemical kinetics [6], NO_x [7] and soot formation [8], and turbulent flame speed [9], along with high-pressure combustion [10]. This paper focuses on the limit phenomena of stability and extinction of diffusion flames, which are highly relevant to ammonia combustion systems due to the low reactivity of NH_3. The stability of diffusion flames is dictated by the Damköhler number (Da), the ratio of the characteristic residence time over the reaction time, as per the well-known S-shape response curve. At the Burke-Schumann limit ($D_a \rightarrow \infty$), combustion is intense and stable. However, when the characteristic reaction time is comparable to the residence time, the flame becomes intrinsically unstable and prone to extinction [11].

* Corresponding author at: Department of Mechanical Engineering, McGill University, 817 Sherbrooke Street West, Montreal, Quebec H3A 0C3, Canada.
E-mail address: elie.antar@mail.mcgill.ca (E. Antar).

https://doi.org/10.1016/j.proci.2026.106214
Received 15 March 2026; Accepted 7 June 2026
Available online 7 July 2026
1540-7489/© 2026 The Authors. Published by Elsevier Inc. on behalf of The Combustion Institute. This is an open access article under the CC BY-NC-ND license (http://creativecommons.org/licenses/by-nc-nd/4.0/).

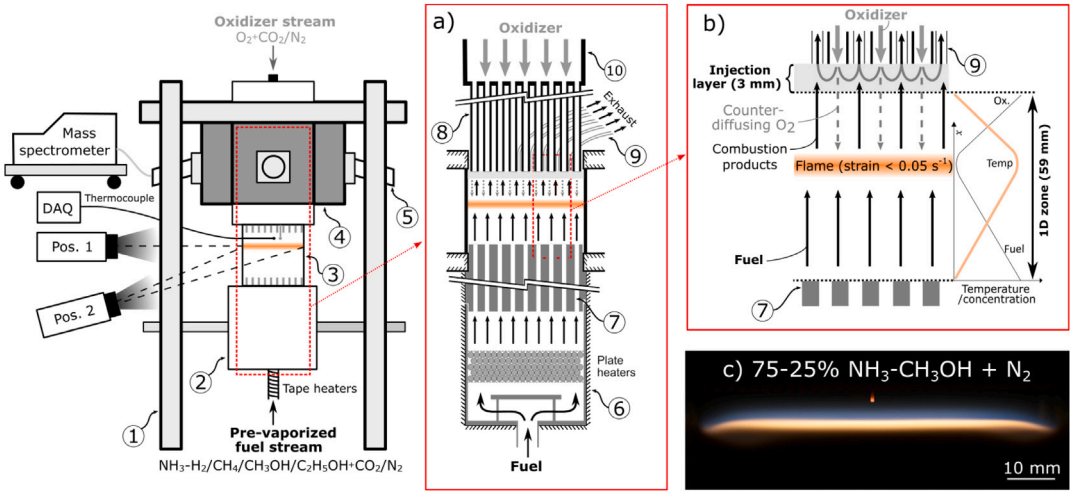

Fig. 1. Schematic representation of the unstrained diffusion flame burner showing (a) its cross-sectional view, (b) the 1D zone, and (c) a horizontal view image of a 75–25% NH_3–CH_3OH flame. (1) Burner support; (2) fuel injection plenum; (3) optically accessible combustion chamber (77.5 × 77.5 mm cross-section); (4) extraction plenum; (5) exhaust tube; (6) fuel mixing chamber; (7) fuel injection block with 18 × 18 2-mm holes; (8) oxidizer injection 31 × 31 needles array (I.D. 1.0 mm); (9) extraction 32 × 32 needles array (I.D. 1.2 mm); and (10) oxidizer mixing chamber.

While cellular instabilities in premixed NH_3 flames have been investigated [12], intrinsic flame instabilities in diffusion NH_3 flames remain largely unexplored [13]. Contrary to premixed flames, the Darrieus–Landau instability plays a secondary role in non-premixed flames, which are primarily driven by diffusive–thermal effects that result in cellular patterns at small Lewis numbers and pulsating instabilities at large Lewis numbers [14]. The scarcity in NH_3 diffusion flame instability data is perhaps a consequence of the nature of commonly used research burners, which involve multidimensional strained or sheared flows that are non-trivial to decouple from the intrinsic flame instabilities [14]. Experimental facilities producing flames subjected to minimal parasitic hydrodynamic effects are needed.

Unlike the dynamics of flame instabilities, the extinction limits of NH_3 diffusion flames have been studied on several occasions using counterflow burners in which extinction is attained by systematically increasing the strain rate, which reduces the residence time in the flame zone. Besides their practical importance in the design of efficient combustors, experimental data on finite-rate chemistry phenomena, such as extinction, serve as valuable tools for the validation of NH_3 thermochemical reaction mechanisms, as shown in Colson et al. [15], Alfazazi et al. [16], Murakami et al. [17] and Thomas et al. [18]. However, in contrast to the relatively well-documented strain-induced extinction limits in these studies, data on dilution-induced extinction are scarce. Dilution with inert species renders the flame prone to extinction by increasing the characteristic chemical reaction time. Besides their importance for emission reduction strategies, dilution-induced extinction limits would expand the existing experimental dataset for the development of more robust NH_3 thermochemical mechanisms, which are still associated with significant levels of uncertainty.

Thus, based on the two research gaps identified above, the goal of this paper is to characterize the intrinsic combustion instabilities and determine the dilution-induced extinction limits of a wide range of NH_3–H_2, NH_3–CH_4, NH_3–CH_3OH, and NH_3–C_2H_5OH diffusion flames. An intricate experimental facility that can generate nominally unstrained diffusion flames, devoid of significant hydrodynamic effects, is used. The simplicity of this flame configuration enables analytical treatment of limit phenomena, permitting fundamental insights into the characteristics of NH_3 flame instabilities, and comparing the new extinction limit measurements with different thermochemical mechanisms.

2. Experimental facility

Fig. 1 shows a schematic representation of the experimental facility used to create 1D, unstrained diffusion flames. This configuration emulates the classical chambered diffusion flame theoretical construct with an upward bulk flow [19]. The combustion chamber is a square duct, supplied with fuel from the bottom and exposed to constant conditions at the top oxidizer side. Oxygen counter-diffuses downward against the bulk flow of the combustion products to reach the flame, which is unstrained as the flow is 1D and uniform throughout the combustion chamber.

The burner was originally introduced by Jacono et al. [20], upgraded by Robert and Monkewitz [21] to reduce the residual strain rate below $0.05\ s^{-1}$, and recently updated by Antar and Robert [22] to accommodate liquid fuels. Details on the burner design and operation can be found in these papers, and only a summary is provided here. A perforated aluminum block is used to uniformly supply the fuel from the bottom of the combustion chamber, while the oxidizer is supplied from the top using numerous thin capillaries, between which the products escape, as shown in Fig. 1(a). The injected oxidizer species initially mix with the bulk flow of products in a locally 3D flow field, referred to as the injection layer (~3 mm thick), below which they counter-diffuse downward toward the flame in a nominally 1D flow field, as confirmed by Laser Doppler anemometry (LDA) and mass spectroscopy [21]. Therefore, 1D conditions that mimic the idealized chambered diffusion flame are achieved over an effective length of $62 - 3 = 59$ mm (Fig. 1b).

Upstream of the burner, NH_3 is mixed with H_2, CH_4, or pre-vaporized alcohols (CH_3OH or C_2H_5OH). The fuel is then diluted with N_2 or CO_2 and supplied into the combustion chamber at the desired inlet velocity (U) and a fixed temperature of 140°C. Details on the fuel vaporization and mixing system can be found in [22]. A calibrated mass spectrometer [23] is used to measure the species concentration at the top of the combustion zone. The species concentrations cannot be determined simply from the injected oxidizer stream, as a fraction of the supplied O_2 is directly evacuated with the products and does not make it beyond the injection layer (Fig. 1b). A type-R thermocouple is used to measure the temperature at the top boundary. The probe is ceramic-coated and inserted horizontally into the combustion chamber to minimize catalytic effects and conduction losses from the vertical temperature gradient.

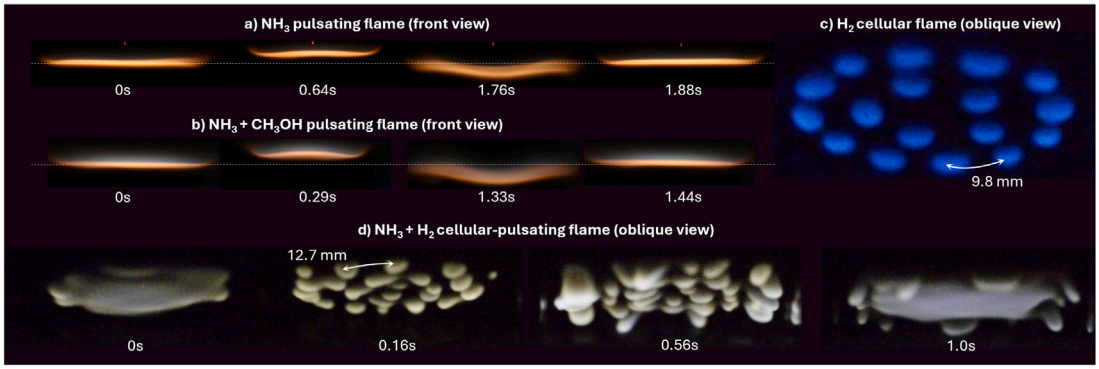

Fig. 2. (a) Front view of a pulsating NH_3 flame, (b) front view of a pulsating 75-25% NH_3–CH_3OH flame, (c) oblique view of a cellular H_2 flame, and (d) oblique view of a 12.5–87.5% NH_3H_2 cellular-pulsating flame.

3. Flame instabilities

The linear stability analysis of the general asymptotic theory of diffusion flames by Cheatham and Matalon [24] applied to 1D unstrained flow conditions yields a dispersion relation that dictates the characteristics of flame instabilities, which are, to the first order, governed by $Le_F, Le_O, \phi, \Delta T$, and D_a. Le_F and Le_O are the fuel and oxidizer Lewis numbers, respectively, which are both important in non-premixed systems. The Lewis number is computed as $Le = D_{th}/D$, with D_{th} being the thermal diffusivity of the mixture, and D the mixture-averaged molecular diffusivity of the species of interest, both evaluated in the flame zone using the model described in [22] and used in Section 5. In this study, the value of $Le_O \approx 1.05$ does not vary significantly across the different flames studied. This is unlike Le_F, which is computed by weighing the Lewis number of each fuel species by its molar fraction relative to the other combustible species in the blend, as in [22]. ϕ is an equivalence ratio based on the fuel and oxidizer supply conditions, referred to as the initial mixture strength [25]. It is computed as the stoichiometry-normalized ratio of the fuel to oxidizer mass fractions at their respective boundaries. ΔT is the temperature difference between the fuel and oxidizer boundaries, kept roughly constant in this study.

Experimentally, flame instabilities are triggered by gradually increasing the dilution levels starting from a stable flame. The type of instability is largely dictated by the fuel composition. Planar intensity pulsations are observed in NH_3 flames, as shown in Fig. 2(a). Pulsating instabilities onset at large Lewis numbers, which are plotted in Fig. 3, and manifest as temporal variations in the reaction rate, causing the flame position to oscillate. The pulsations occur at well-defined frequencies, which are extracted from the flame videos as detailed in [22], and plotted in Fig. 4. The pulsating frequencies are normalized by the characteristic flow time, $t_{flow} = D_{th}/U_f^2$, with U_f being the bulk velocity through the flame. The measured pulsation frequency increases with mixture strength, consistent with theoretical predictions [26].

While CH_3OH, and C_2H_5OH fuels also exhibit pulsating instabilities, as well as CH_4 which was analyzed in our previous work [13], their addition to NH_3 increases the pulsation frequency as shown in Fig. 2(b) and Fig. 4. The oscillations become faster also upon replacing CO_2 dilution with N_2, as shown by the gray symbols of Fig. 4. These trends are fundamentally driven by the fuel Lewis number. As seen from Fig. 4, the pulsation frequency of flames burning different fuels scales the same if their Lewis number is similar.

Another type of instability, cellular flames, is observed with hydrogen fuels, as shown in Fig. 2(c). Cellular instabilities manifest as spatial variation in heat production, fragmenting the flame into multiple local hot spots. Cellular instabilities onset at small Lewis numbers, which is typical for hydrogen flames as shown in Fig. 3. The fundamental characteristics of hydrogen cellular instabilities, such as cell size, have been studied previously by Robert and Monkewitz [27], and are consistent with theoretical predictions. Interestingly, when mixing low and high Le fuels, such as H_2 + NH_3, cellular and pulsating instabilities co-exist in the flame, as shown in Fig. 2(d). Cells appear at the lowest intensity point of the pulsation cycle ($t = 0.16$ s), which grow in amplitude before merging together near the peak of the pulsation wave ($t = 1.0$ s), where a planar flame is momentarily reestablished, before the repetition of the cycle. The fundamental properties of these peculiar instabilities are discussed in a dedicated publication [13].

4. Extinction limits

Fig. 5 shows the experimentally measured extinction limits in terms of the total fuel fraction (mole fraction of all fuel species relative to inert, X_F). The raw data are provided in the supplementary material. Starting from a stable flame, X_F is gradually reduced in 0.25% decrements until extinction is observed. Extinction was marked by an abrupt and clear disappearance of chemiluminescence, which was followed by a sharp change in the measured species concentrations at the top oxidizer side. It is observed that increasing the fraction of NH_3 relative to the other fuel species (X_{NH_3}) significantly favors extinction. For instance, with CO_2 dilution (solid symbols), the extinction limit goes from X_F = 10.0% to 15.75% when 50% NH_3 is added to CH_4, and eventually becomes X_F = 35.75% for a 100% NH_3 flame (Fig. 5b). Blending NH_3 with C_2H_5OH provides the most ability to extend the flammability limits (Fig. 5d), followed by CH_4 (Fig. 5b), CH_3OH (Fig. 5c), and H_2 (Fig. 5a). For example, with CO_2 dilution, to avoid extinction at a total fuel concentration of 17.5%, approximately 20% C_2H_5OH has to be blended with NH_3, which increases to 37% with CH_4, 50% with CH_3OH, and all the way up to 100% with H_2 (NH_3-free). This correlates with the molar HHV of the fuels, and thus, the characteristic combustion temperatures, with C_2H_5OH being the highest at 1368 MJ/kmol followed by CH_4 at 890 MJ/kmol, CH_3OH at 737 MJ/kmol, and H_2 at 286 MJ/kmol.

While the trends are similar to CO_2 dilution, it can be seen in Fig. 5 (open symbols) that the flammability limits are wider, *i.e.* exhibit lower overall X_F values, with N_2. Data for N_2-diluted NH_3–H_2 flames are limited to $X_{NH_3} \geq 37.5\%$ as cellular flame instabilities hinder the reliable determination of the extinction limits at high hydrogen fractions. To shed light on the different dilution effects of CO_2 and N_2, commonly categorized as inert, thermal/diffusion, and chemical effects [28], a 1D chambered non-premixed flame numerical model is implemented in Python using the Cantera software package [29]. Details of the flame model can be found in Antar and Robert [22], which is also used for the kinetic modeling results discussed in the next section. The 50–50% NH_3–CH_4 case is considered, and four artificial inert species (XNH_3, XCH_4, XCO_2 and XN_2) are introduced into the mechanism by Okafor et al. [30]. These artificial species do not participate in the chemical reactions, but have the same thermodynamic and transport properties as their reactive counterparts. On the oxidizer side, the temperature is set at 1127°C, and the species concentrations are such that $\phi = 1.0$.

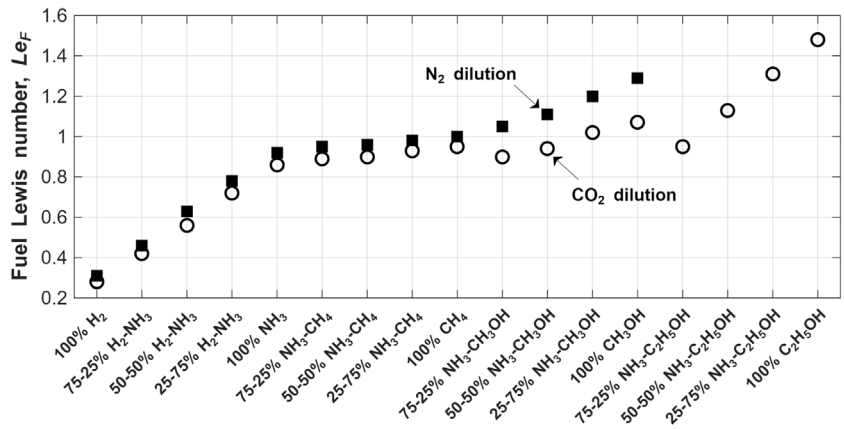

Fig. 3. Fuel Lewis number of the different flames studied.

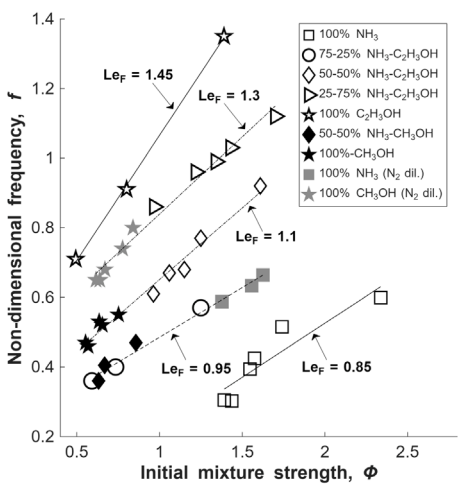

Fig. 4. Scatter plot of the non-dimensional pulsation frequency for different NH_3 fuel blends. CO_2 is used as inert, except for the gray symbols where N_2 is used.

Starting with the inert effect, a 50–50% XNH_3-XCH_4 diluent is used, and extinction is attained at X_F = 11%. This simply illustrates the consequence of reducing the reactants concentration, with the diluent having the same thermal and diffusive properties as the fuel (50–50% NH_3–CH_4). To isolate the effect of changing the thermal and transport properties of the mixture when diluting with CO_2, *i.e.* thermal/diffusion effect, XCO_2 is used as a diluent, which advances extinction to X_F = 11.5%. The thermal/diffusion effect of N_2 dilution, on the other hand, significantly delays extinction to X_F = 6.25%, and increases the flame temperature mainly because of the lower volumetric heat capacity of N_2 compared to CO_2. Finally, upon incorporating CO_2 in the chemical reactions, extinction is further advanced to X_F = 13.25%, while negligible differences in the extinction limit and flame temperature are reported when incorporating reactive N_2 species compared to XN_2. Hence, the extended extinction limits of N_2-diluted flames compared to CO_2 diluted ones in Fig. 5 can be attributed to the thermal/diffusion properties of N_2 and chemical effects of CO_2. Similar dilution effects were also reported in syngas, non-premixed flames diluted in CO_2 and N_2 [28].

To better understand these effects, sensitivity and reaction pathway [31] analyses are presented in Figs. 6 and 7. Interestingly, the sensitivities with nitrogen or carbon dioxide in the fuel mixture are similar, which supports the affirmation above that the main cause for the shift in the extinction limit is the higher flame temperature with N_2, which increases the rate of the reactions. Furthermore, only a few reactions have a significant impact on the extinction limit, two of which feature carbon dioxide (blue dashed box). Replacing CO_2 by inert XCO_2 in the fuel blend presumably favors the exothermic conversion of CO into carbon dioxide through the reactions $CO + OH \leftrightarrow CO_2 + H$ and $CH_{2(S)} + CO_2 \leftrightarrow CH_2O + CO$, which hinders extinction (chemical effect identified above). In contrast, N_2 behaves as an inert third body in a few key reactions, which explains that replacing N_2 by its inert counterpart XN_2 has a minimal impact on the extinction limit.

The RPAs presented in Fig. 7 are remarkably similar with N_2 (solid arrows) and CO_2 (dashed arrows) dilution, both in terms of the relative rate of heat production and fraction of hydrogen atoms through the individual paths. This confirms the limited impact of the diluent on the chemistry, and supports that the main effect leading to lower values of X_F at extinction with N_2 dilution is the higher flame temperature. It is also worth noticing that an increasing fraction of the hydrogen atoms are diverted from the methane oxidation route toward the hydrogen abstraction pathway ($NH_3 \rightarrow NH_2 \rightarrow NH$) as the fraction of ammonia in the fuel mixture rises. Since extinction is favored at higher ammonia fractions, this implies that its chemistry is slower than the other fuel (H_2, CH_4, CH_3OH or C_2H_5OH) in the blends.

5. Kinetic modeling

Eleven common thermochemical reaction mechanisms are evaluated for the first time in the unstrained diffusion flame configuration: Gas Research Institute (GRI3.0, 53 species and 325 reactions), Okafor et al. [30] (Okafor2018, 59 species and 356 reactions), University of California - San Diego [32] (UCSD, 68 species and 311 reactions), Wang et al. [33] (Wang2021, 91 species and 444 reactions), Kovaleva et al. [34] (Kovaleva2022, 59 species and 354 reactions), Thomas et al. [18] (Thomas2023, 125 species and 1099 reactions), Mie et al. [35] (Mie2021, 40 species and 257 reactions), Stagni et al. [36] (POLIMI2020, 31 species and 210 reactions), Han et al. [37] (Han2019, 35 species and 177 reactions), Zhang et al. [38] (Zhang2021, 38 species and 263 reactions), and the reduced mechanism by Shrestha et al. [39] (Shrestha2025, 38 species and 307 reactions).

Fig. 5(a) presents the extinction limits predicted by different mechanisms for NH_3–H_2 blends. For CO_2 dilution, the results by the Wang2021 model is the closest to the experimental data. The Okafor2018 mechanism yields similar values to Wang2021 for intermediate NH_3 fractions (X_{NH_3} < 75%), while UCSD, Thomas2023, and Kovaleva2022 consistently underpredict extinction. Despite being in agreement with the experiments for moderate X_{NH_3}, GRI3.0 produces an inconsistent dip at low NH_3 fractions. With N_2 dilution,

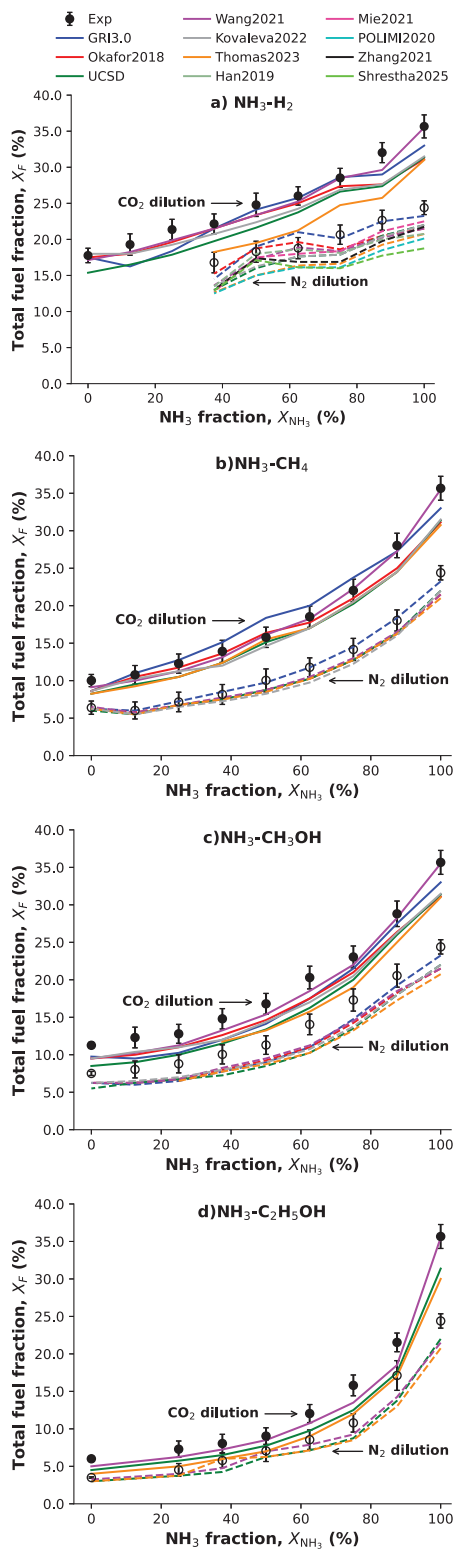

Fig. 5. Measured extinction limits and modeling predictions for NH_3–H_2/CH_4/CH_3OH/C_2H_5OH at U = 18.9 mm/s. Open symbols and dashed lines represent N_2 dilution. Error bars include the range of repeated measurements.

Okafor2018 provides the best agreement for intermediate X_{NH_3}, while GRI3.0 prevails at $X_{NH_3} \geq 75\%$. POLIMI2020, Thomas2023, UCSD, Kovaleva2022, and Mie2021 constantly underpredict extinction, but

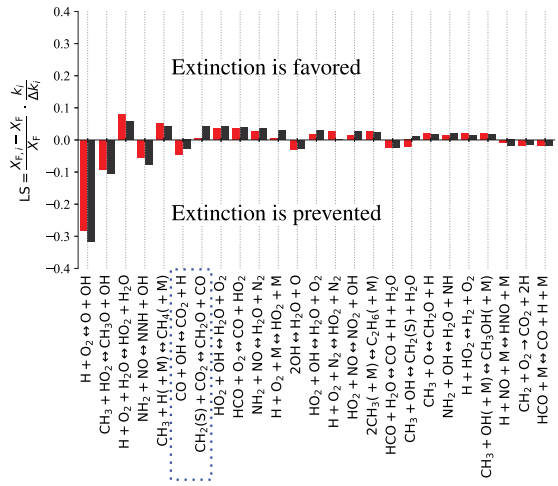

Fig. 6. Logarithmic sensitivity (LS) of the fuel mole fraction at extinction to the rate of the reactions for a 50–50% NH_3–CH_4 fuel blend diluted with N_2 (red) and CO_2 (black) modeled with the mechanism by Okafor et al. [30]. The 25 reactions with the largest LS are shown.

are able to replicate the experimental trend, unlike the rest of the mechanisms which exhibit an incorrect dip at X_{NH_3} = 75%.

Fig. 5(b) compares the predicted and experimental extinction limits for NH_3–CH_4 blends. While the trends are consistent for the different mechanisms for CO_2 dilution, the absolute values of the extinction limits differ. UCSD and Thomas2023 underpredict extinction at low and high X_{NH_3} values, wheres GRI3.0 overpredicts extinction at moderate X_{NH_3}. Although the Okafor2018 mechanism is in quantitative agreement with the experimental data for $X_{NH_3} \leq 75\%$, the Wang2021 mechanism provides the best agreement with the experiments across all NH_3 fractions. Considering N_2-diluted blends, it can be seen that the predictions from all mechanisms are within the experimental uncertainty with the exception of high NH_3 fractions, $X_{NH_3} > 75\%$. Similar to CO_2 dilution, GRI3.0 predicts the highest extinction total fuel fraction.

Fig. 5(c) shows the extinction limits of NH_3–CH_3OH blends predicted by the different mechanisms. The monotonically increasing experimental trend is captured by all models. As with previous CO_2-diluted blends, the extinction limits by the Wang2021 mechanism agree best with the experiments, although underpredictions are observed at high CH_3OH content. When diluting with N_2, all mechanisms underpredict the extinction limits, with Wang2021 being the closest to the experimental data followed by Okafor2018.

Fig. 5(d) presents the extinction limits of NH_3–C_2H_5OH blends. It can be seen that the Wang2021 model agrees reasonably well with the experimental data for both CO_2 and N_2 dilution. While the trends are consistent with the experiments, UCSD and Thomas2023 underpredict extinction, with the exception of low X_{NH_3} values for N_2-diluted blends. The rest of the mechanisms are excluded since they do not incorporate C_2H_5OH. Based on an overall error computed across all fuel blends (supplementary material), the Wang2021 model shows the best agreement with the experimental data, followed by Okafor2018.

6. Conclusion

The limit phenomena of flame stability and extinction are investigated for more than 70 distinct NH_3–H_2/CH_4/CH_3OH/C_2H_5OH fuel blends diluted in either CO_2 or N_2. A unique burner that can produce nominally 1D unstrained diffusion flames, devoid of the parasitic hydrodynamic effects present in common research burners, is used to observe and gain fundamental insight into the diffusive–thermal flame instabilities that onset near extinction. Pulsating flames are observed with NH_3, whose frequency increases with the addition of CH_4, CH_3OH,

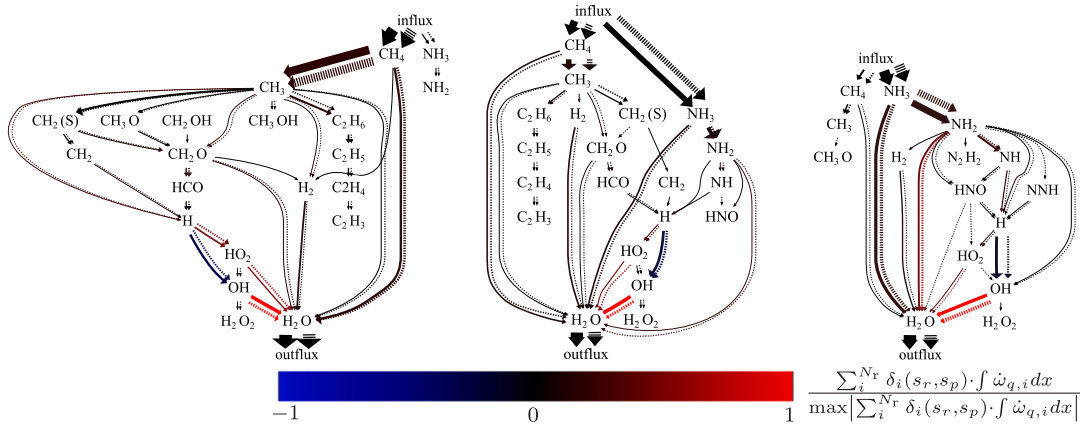

Fig. 7. Reaction pathway diagrams tracking the flux of hydrogen atoms for 12.5–87.5% (left), 50–50% (center) and 87.5–12.5% (right) NH_3–CH_4 fuel mixtures. Only pathways transporting >3% of the H atoms are shown. The solid and dashed arrows correspond to flames diluted with N_2 and CO_2, respectively, and are colored by the relative rate of heat production of the individual paths ($\dot{\omega}_{q,i}$ is the volumetric rate of heat production by reaction i, N_r is the number of chemical reactions, and $\delta_i\left(s_r, s_p\right)$ equals 1 if the reaction i involves both species forming the path (s_r and s_p), and 0 otherwise). The flames were simulated with a value of X_F 0.25% higher than extinction.

or C_2H_5OH, as the Lewis number becomes larger. Hydrogen fuel blends, which have small Lewis numbers, produce cellular instabilities that co-exist with pulsating instabilities when mixed with NH_3.

The finite-rate chemistry of extinguishing flames is leveraged to compare 11 frequently used thermochemical reaction mechanisms with experimental measurements. While most models are able to qualitatively reproduce the experimental trends, significant discrepancies between the models remain when it comes to the absolute values of the extinction limits. The experimental data presented in this paper, therefore, also establish a new benchmark for improving ammonia reaction mechanisms, providing a foundation for their systematic refinement and validation.

CRediT authorship contribution statement

Elie Antar: Performed research, Analyzed data, Wrote paper. **Philippe Versailles:** Performed research, Analyzed data, Wrote paper. **Etienne Robert:** Analyzed data, Reviewed paper, Secured funding.

Declaration of competing interest

The authors declare that they have no known competing financial interests or personal relationships that could have appeared to influence the work reported in this paper.

Acknowledgments

The Trottier Energy Institute (scholarship and project grant), Natural Sciences and Engineering Research Council of Canada (NSERC) (scholarship PGSD3-546588–2020, and discovery grants RGPIN-03622-2014 and RGPIN-05071-2022), and Fonds de Recherche du Québec Nature et technologies (FRQNT) (B2X scholarship).

Appendix A. Supplementary data

Supplementary material related to this article can be found online at https://doi.org/10.1016/j.proci.2026.106214.

References

[1] H. Kobayashi, A. Hayakawa, K.K.A. Somarathne, E.C. Okafor, Science and technology of ammonia combustion, Proc. Combust. Inst. 37 (2019) 109–133.
[2] A.M. Elbaz, S. Wang, T.F. Guiberti, W.L. Roberts, Review on the recent advances on ammonia combustion from the fundamentals to the applications, Fuel Commun. 10 (2022) 100053.
[3] C.D. Ávila, S. Cardona, M. Abdullah, M. Younes, A. Jamal, T.F. Guiberti, W.L. Roberts, Experimental assessment of the performance of a commercial micro gas turbine fueled by ammonia-methane blends, Appl. Energy Combust. Sci. 13 (2023) 100104.
[4] S. Zitouni, P. Brequigny, C. Mounam-Rousselle, Influence of hydrogen and methane addition in laminar ammonia premixed flame on burning velocity, Lewis number and Markstein length, Combust. Flame 253 (2023) 112786.
[5] W.S. Chai, Y. Bao, P. Jin, G. Tang, L. Zhou, A review on ammonia, ammonia-hydrogen and ammonia-methane fuels, Renew. Sustain. Energy Rev. 147 (2021) 111254.
[6] J. Chen, X. Gou, Experimental and kinetic study on the extinction characteristics of ammonia-dimethyl ether diffusion flame, Fuel 334 (2023) 126743.
[7] G. Wang, H. Tang, C. Yang, G. Magnotti, W.L. Roberts, T.F. Guiberti, Quantitative laser-induced fluorescence of NO in ammonia-hydrogen-nitrogen turbulent jet flames at elevated pressure, Proc. Combust. Inst. 39 (2023) 1465–1474.
[8] M.H. Zaher, M. Dadsetan, C. Chu, M.J. Thomson, The effect of ammonia addition on soot nanostructure and composition in ethylene laminar flames, Combust. Flame 251 (2023) 112687.
[9] S. Zitouni, P. Brequigny, C. Mounam-Rousselle, Turbulent flame speed and morphology of pure ammonia flames and blends with methane or hydrogen, Proc. Combust. Inst. 39 (2) (2023) 2269–2278.
[10] A.A. Khateeb, T.F. Guiberti, G. Wang, W.R. Boyette, M. Younes, A. Jamal, W.L. Roberts, Stability limits and NO emissions of premixed swirl ammonia-air flames enriched with hydrogen or methane at elevated pressures, Int. J. Hydrog. Energy 46 (21) (2021) 11969–11981.
[11] P. Metzener, M. Matalon, Diffusive-thermal instabilities of diffusion flames: onset of cells and oscillations, Combust. Theory Model. 10 (2006) 701–725.
[12] H. Li, H. Xiao, J. Sun, Laminar burning velocity, Markstein length, and cellular instability of spherically propagating NH_3/H_2/Air premixed flames at moderate pressures, Combust. Flame 241 (2022) 112079.
[13] E. Antar, E. Robert, Intrinsic combustion instabilities in ammonia-hydrogen/methane non-premixed flames, Proc. Combust. Inst. 40 (2024) 105203.
[14] M. Matalon, Intrinsic flame instabilities in premixed and nonpremixed combustion, Annu. Rev. Fluid Mech. 39 (2007) 163–191.
[15] S. Colson, Y. Hirano, A. Hayakawa, T. Kudo, H. Kobayashi, C. Galizzi, D. Escudié, Experimental and numerical study of NH_3/CH_4 counterflow premixed and non-premixed flames for various NH_3 mixing ratios, Combust. Sci. Technol. 193 (2021) 2872–2889.
[16] A. Alfazazi, E. touhami Es-sebbar, X. Zhang, B. Dally, M. Abdullah, M. Younes, S.M. Sarathy, Counterflow flame extinction of ammonia and its blends with hydrogen and C_1-C_3 hydrocarbons, Appl. Energy Combust. Sci. 12 (2022) 100099.
[17] Y. Murakami, T. Tezuka, H. Nakamura, The extinction limits and the radical index of non-premixed counterflow flames of methane/ammonia/nitrogen versus high-temperature air, Combust. Flame 266 (2024) 113540.

[18] D.E. Thomas, K.P. Shrestha, F. Mauss, W.F. Northrop, Extinction and NO formation of ammonia-hydrogen and air non-premixed counterflow flames, Proc. Combust. Inst. 39 (2023) 1803–1812.
[19] L. Kirkbey, R. Schmitz, An analytical study of the stability of a laminar diffusion flame, Combust. Flame 10 (1966) 205–220.
[20] D. Lo Jacono, P. Papas, M. Matalon, P. Monkewitz, An experimental realization of an unstrained, planar diffusion flame, Proc. Combust. Inst. 30 (2005) 501–509.
[21] E. Robert, P.A. Monkewitz, Experimental realization and characterization of unstretched planar one-dimensional diffusion flames, Combust. Flame 160 (2013) 546–556.
[22] E. Antar, E. Robert, Diffusive-thermal instabilities in unstrained H_2O-diluted syngas diffusion flames, Combust. Flame 261 (2024) 113313.
[23] E. Robert, Mass spectrometer calibration over wide concentration ranges in multicomponent gas mixtures, Meas. Sci. Technol. 21 (2010) 025102.
[24] S. Cheatham, M. Matalon, A general asymptotic theory of diffusion flames with application to cellular instability, J. Fluid Mech. 414 (2000) 105–144.
[25] E. Antar, J. Delavande, E. Robert, Experimental characterization of diffusive-thermal instabilities in CO2-diluted H2CH4CO unstrained diffusion flames, Combust. Flame 250 (2023) 112636, https://www.sciencedirect.com/science/article/pii/S0010218023000214, https://doi.org/10.1016/j.combustflame.2023.112636.
[26] S. S. Kukuck, M. Matalon, The onset of oscillations in diffusion flames, Combust. Theory Model. 5 (2001) 217–240.
[27] E. Robert, P.A. Monkewitz, Thermal-diffusive instabilities in unstretched, planar diffusion flames, Combust. Flame 159 (2012) 1228–1238.
[28] H.-Y. Shih, J.-R. Hsu, Y.-H. Lin, Computed flammability limits of opposed-jet H_2/CO syngas diffusion flames, Int. J. Hydrog. Energy 39 (2014) 3459–3468.
[29] D.G. Goodwin, H.K. Moffat, I. Schoegl, R.L. Speth, B.W. Weber, Cantera: An object-oriented software toolkit for chemical kinetics, thermodynamics, and transport processes, 2023.
[30] E.C. Okafor, Y. Naito, S. Colson, A. Ichikawa, T. Kudo, A. Hayakawa, H. Kobayashi, Experimental and numerical study of the laminar burning velocity of CH_4–NH_3–air premixed flames, Combust. Flame 187 (2018) 185–198.
[31] J.F. Grcar, M.S. Day, J.B. Bell, A taxonomy of integral reaction path analysis, Combust. Theory Model. 10 (4) (2006) 559–579.
[32] Chemical-Kinetic Mechanisms for Combustion Applications, San Diego Mechanism web page, Mechanical and Aerospace Engineering (Combustion Research), University of California at San Diego (http://combustion.ucsd.edu).
[33] Z. Wang, X. Han, Y. He, R. Zhu, Y. Zhu, Z. Zhou, K. Cen, Experimental and kinetic study on the laminar burning velocities of NH_3 mixing with CH_3OH and C_2H_5OH in premixed flames, Combust. Flame 229 (2021) 111392.
[34] M. Kovaleva, A. Hayakawa, S. Colson, E.C. Okafor, T. Kudo, A. Valera-Medina, H. Kobayashi, Numerical and experimental study of product gas characteristics in premixed ammonia/methane/air laminar flames stabilised in a stagnation flow, Fuel Commun. 10 (2022) 100054.
[35] B. Mei, S. Ma, X. Zhang, Y. Li, Characterizing ammonia and nitric oxide interaction with outwardly propagating spherical flame method, Proc. Combust. Inst. 38 (2021) 2477–2485.
[36] A. Stagni, C. Cavallotti, S. Arunthanayothin, Y. Song, O. Herbinet, F. Battin-Leclerc, T. Faravelli, An experimental, theoretical and kinetic-modeling study of the gas-phase oxidation of ammonia, React. Chem. Eng. 5 (2020) 696–711.
[37] X. Han, Z. Wang, M. Costa, Z. Sun, Y. He, K. Cen, Experimental and kinetic modeling study of laminar burning velocities of NH_3/air, NH_3/H_2/air, NH_3/CO/air and NH_3/CH_4/air premixed flames, Combust. Flame 206 (2019) 214–226.
[38] X. Zhang, S.P. Moosakutty, R.P. Rajan, M. Younes, S.M. Sarathy, Combustion chemistry of ammonia/hydrogen mixtures: Jet-stirred reactor measurements and comprehensive kinetic modeling, Combust. Flame 234 (2021) 111653.
[39] K.P. Shrestha, B.R. Giri, R. Pelé, K. Aljohani, P. Brequigny, F. Mauss, F. Halter, L.K. Huynh, C. Mounaïm-Rousselle, A comprehensive chemical kinetic modeling and experimental study of NH_3-methanol/ethanol combustion towards net-zero CO_2 emissions, Combust. Flame 274 (2025) 113954.